atmosphere

MDPI

Article

Evaluating and Merging Satellite and Reanalysis Precipitation Products with Station Observations Using XGBoost in the Jinsha River Basin, China

Ye Yin [1], Hantao Wang [1], Hui Zhang [1,*], Nanshan Zhao [1], Cuihua Cheng [1] and Chenghua Xie [2]

[1] The Three Gorges Jinsha River Chuanyun Hydropower Development Co., Ltd., China Yangtze Power Co., Ltd., Chengdu 610025, China
[2] Chengdu Yuanwang Detection Technology Co., Ltd., Chengdu 610025, China
* Correspondence: zhang_hui7@ctg.com.cn

Abstract

The Jinsha River Basin constitutes the largest hydropower base in China. However, its complex terrain results in insufficient accurate data support for numerical forecasts, leading to low accuracy in precipitation predictions. To investigate the spatiotemporal distribution characteristics of precipitation in this basin with high precision, we evaluated the applicability of several mainstream precipitation products—GSMAP (Global Satellite Mapping of Precipitation), GPM-IMERG (Integrated Multi-satellite Retrievals for Global Precipitation Measurement), CMORPH (Climate Prediction Center Morphing technique), and ERA5 (European Center for Medium-Range Weather Forecasts Reanalysis 5)—in the Jinsha River Basin. Based on the XGBoost algorithm, we developed a merging model that integrates satellite and reanalysis data with station observations for daily-scale applications. The results indicate that the GSMAP-Gauge precipitation product exhibits strong performance in both quantitative accuracy and precipitation event detection, with a better correlation coefficient (CC = 0.66), the lowest root mean square error (RMSE = 4.45), and higher probability of detection (POD = 0.88) and critical success index (CSI = 0.59). The ERA5 and GSMAP-Gauge products performed well in detecting light rain events (daily precipitation < 10 mm), with hit rates of 0.92 and 0.90, respectively. Meanwhile, the GPM-IMERG and CMORPH-BLD products showed higher hit rates for heavy rain events (daily precipitation > 25 mm) compared to the other two products. Specifically, the POD indices for GPM-IMERG and CMORPH-BLD were 0.45 and 0.60, respectively, while those for ERA5 and GSMAP-Gauge were below 0.4. Following the precipitation merging experiment, the multi-source precipitation merged product (MSP) substantially enhanced the accuracy of precipitation estimates, and the spatiotemporal distribution characteristics of the merged data aligned more closely with the station observations. This study analyzes the strengths and limitations of various precipitation products in the Jinsha River Basin and provides a feasible multi-source precipitation data merging scheme, offering a novel approach to constructing high-precision daily precipitation datasets in complex terrain regions.

Keywords: applicability assessment; machine learning; data merging

Academic Editor: Merhala Thurai

Received: 6 May 2026
Revised: 9 June 2026
Accepted: 14 June 2026
Published: 17 June 2026

1. Introduction

Precipitation is a critical component of the regional hydrological cycle and plays a significant role in climate change, water resources development and management, and disaster warning and monitoring [1]. However, against the backdrop of global warming,

the spatiotemporal patterns of precipitation have shifted, and the frequency of extreme precipitation events has increased, complicating comprehensive meteorological observation due to environmental constraints such as alpine mountains, permafrost, and glaciers [2,3].

Currently, precipitation data are primarily derived from rain gauges, weather radar, and satellite. Although traditional ground-based rain gauges provide high-precision precipitation data, their spatial distribution is limited, particularly in regions with substantial terrain gradients and complex topography, where uneven and sparse station networks directly affect data accuracy [4–7]. Compared with fixed ground stations, weather radar offers superior real-time performance and can rapidly provide continuous spatiotemporal precipitation data. However, due to the challenges of complex mountainous terrain and high deployment costs, radar network distribution remains uneven, making comprehensive coverage of plateau mountainous areas difficult. Additionally, radar-based quantitative precipitation estimation is prone to errors caused by terrain blockage, super-refraction echoes, and bright-band contamination [8,9]. With the rapid development of satellite remote sensing technology, multiple satellite remote sensing datasets are now being used for the continuous spatiotemporal monitoring of weather and climate [10,11]. Satellite remote sensing data, characterized by high spatiotemporal resolution and extensive coverage, have become essential for compensating for the low spatial coverage of ground observations. Wang et al. [12] evaluated the usability of GPM-IMERG data in the Sichuan region using machine learning methods and performed satellite downscaling research. They obtained a high-precision satellite precipitation dataset under Sichuan's complex terrain, effectively compensating for the lack of precipitation observations in complex terrain area. Nevertheless, due to limitations in sensor performance, cloud properties, and retrieval algorithms, satellite precipitation estimates still exhibit considerable errors in practical applications. Numerous studies have evaluated the applicability of various satellite precipitation products across China, particularly in the complex mountainous regions of the Qinghai-Xizang Plateau [13]. For instance, Zeng et al. [14] assessed the accuracy of daily and hourly precipitation data from GPM-IMERG and GSMaP precipitation products in Sichuan, comparing their performance in plateau and basin areas. Their findings revealed that retrieval accuracy was superior in basin areas compared to plateau mountainous regions, with notable differences across terrain types. Xu et al. [15] evaluated the applicability of CHIRPS, GPM-IMERG, and GSMAP satellite precipitation products in the Jinsha River Basin, demonstrating that GSMAP outperformed the other two products across different altitudinal zones. Reanalysis precipitation products were generated by combining historical meteorological observations with numerical models to produce atmospheric datasets with high spatiotemporal resolution. With continuous technological advancements, the accuracy and application scope of reanalysis precipitation products have significantly expanded, and they are now widely used across various fields, including meteorology, hydrology, and environmental science [16,17]. Many researchers have conducted comprehensive evaluations of the accuracy of reanalysis precipitation products. For example, Kidd et al. [18] assessed the reliability of multiple satellite and reanalysis precipitation datasets over northwestern Europe, finding that satellite data exhibited seasonal cycles in metrics such as correlation coefficients and error rates, performing poorly in winter. In contrast, reanalysis data showed only seasonal variation in correlation coefficients, with relatively poor performance during summer. Given that errors are unavoidable across various precipitation products—especially in regions with complex terrain, where the accuracy, coverage, and integrity of different products face significant challenges. It is imperative to conduct a multi-source precipitation product merging test to integrate the strengths of different products, thereby achieving improved precipitation product accuracy.

A growing number of researchers have exploited the advantages of integrating multiple observational data sources to develop a series of multi-source precipitation fusion methods, establishing corresponding precipitation fusion models customized for the characteristics of different study regions. These include geographically weighted regression (GWR) [19], optimum interpolation (OI) [20], and regression Kriging [21]. With the rapid development of machine learning, its robust nonlinear representation capabilities have been effectively utilized in multi-source data merging research. Wu et al. [22] employed a CNN-LSTM approach to perform spatiotemporal deep merging of satellite and station precipitation data across mainland China. Li et al. [23] applied random forest methods to merge and calibrate multi-satellite and reanalysis data in Sichuan Province. These studies demonstrate that machine learning methods can integrate a wider range of precipitation-related information, leading to substantial improvements in precipitation estimation and event detection. However, most existing studies have focused on plains and basins with relatively homogeneous precipitation characteristics. Whether such methods are equally applicable to basins characterized by complex terrain, abundant water flow, and sparse meteorological station networks remains to be determined.

The Yangtze River Basin experiences an uneven distribution of drought and flood, with frequent extreme weather-related disasters. The Jinsha River, in the eastern Qinghai-Xizang Plateau, is the primary source of water and sediment in the upper Yangtze River. It features a large basin area, complex underlying surface conditions, and a sensitive climate [24,25]. The complex plateau terrain has resulted in a sparse and highly uneven spatial distribution of meteorological stations within the Jinsha River Basin. Moreover, errors in the inversion of various satellite datasets, together with uncertainties inherent in reanalysis data sources, impose considerable limitations on the study of precipitation characteristics in complex terrain areas such as the Jinsha River Basin [26,27]. To address these challenges, this study makes the following contributions. Firstly, it systematically evaluates the applicability of four mainstream precipitation products (GPM-IMERG, GSMAP-Gauge, CMORPH-BLD, and ERA5) in the Jinsha River Basin, providing a comprehensive error analysis across multiple timescales and precipitation intensities. Then, it develops a novel multi-source precipitation merging model based on the XGBoost algorithm, which integrates satellite, reanalysis, ground-based station data, and topographic auxiliary parameters (elevation, slope, longitude, latitude) to generate a high-precision daily precipitation dataset at 0.1° spatial resolution. Ultimately, this machine-learning-based approach, tailored to the complex terrain of the Jinsha River Basin, offers a feasible solution for obtaining accurate gridded precipitation data where traditional observations are sparse. The merged dataset provides crucial data support for theoretical research on the evolution of weather systems and for the generation of high-resolution initial fields in numerical models.

2. Study Area and Data

2.1. Study Area

The Jinsha River Basin, located in the upper reaches of the Yangtze River and spanning the Qinghai-Xizang Plateau, is characterized by complex topography with high elevations in the west, lower elevations in the east, and substantial elevation gradients. The upper reaches feature plateau valley landforms with elevations exceeding 4000 m and slow flow velocities. The middle reaches are characterized by alpine canyon landforms, where the river traverses several continuous gorges with elevation differences of 2000–3000 m, resulting in turbulent flow and dense dangerous shoals. The lower reaches are predominantly hilly, with gradually widening water surfaces and decreasing flow velocities [28,29]. The abundant water resources and significant elevation drop provide ideal conditions for hydropower generation, making this region a major hydropower base in China. However, the

complex topography leads to an extremely uneven distribution of meteorological stations and a shortage of precipitation data, thereby hindering the necessary data support for climate change studies and numerical model forecasting in the basin. Accordingly, this study focuses on the Jinsha River Basin. Figure 1 presents the topographic elevation map of the study area.

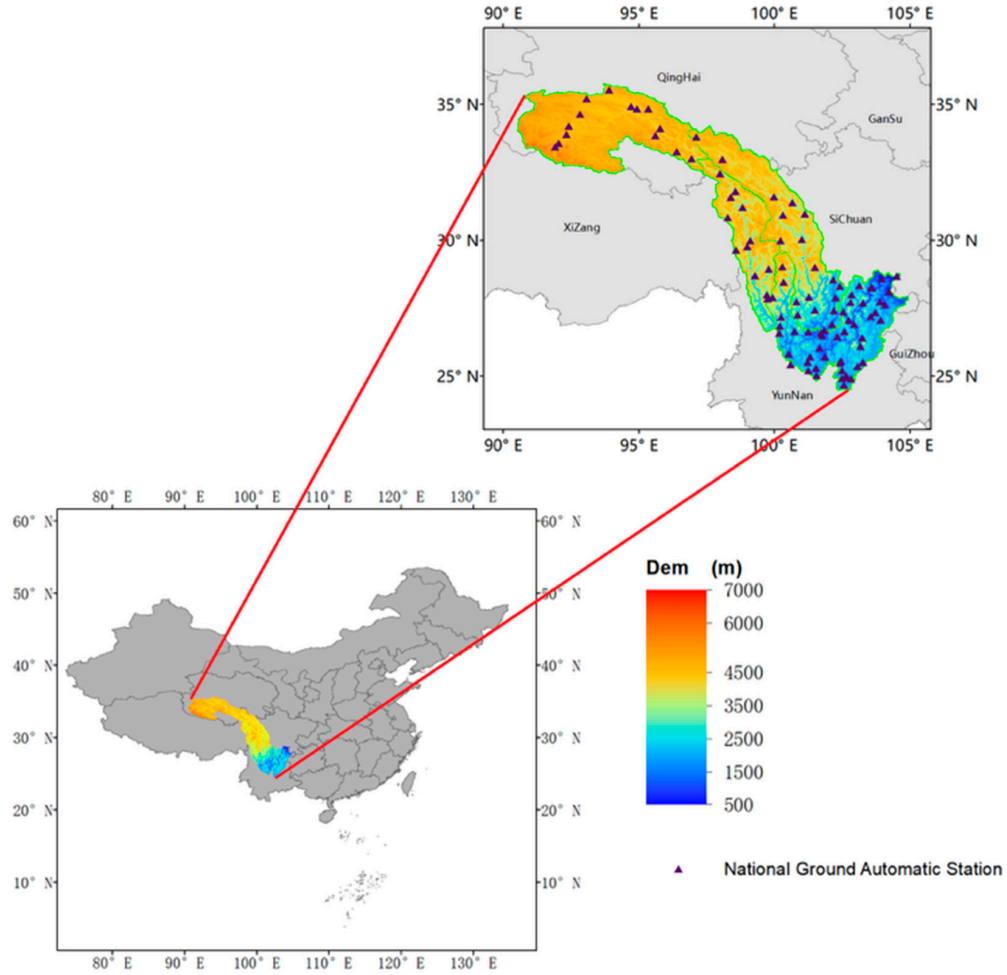

Figure 1. Topographic elevation map of the Jinsha River Basin.

2.2. Data

The data used in this study include GPM-IMERG, GSMAP-Gauge, CMORPH-BLD, and ERA5 precipitation data, as well as precipitation records from over 1800 stations, including regional and national automatic weather stations.

Station-based precipitation observation data offer high accuracy and are often regarded as the reference truth value in data fusion experiments. This study utilized daily precipitation records from more than 1800 automatic weather stations operated by the Sichuan Meteorological Bureau as the station observation data. Station precipitation data from 1 January 2022 to 31 December 2024, within the Jinsha River Basin were selected, and the distribution of national automatic weather stations is shown in Figure 1. To ensure data quality, meteorological stations with more than ten missing days in a single month were excluded from the data quality assessment.

Four mainstream satellite precipitation products and one reanalysis precipitation dataset were selected. The Global Precipitation Measurement (GPM) is a collaborative mission between the National Aeronautics and Space Administration (NASA) and the Japan Aerospace Exploration Agency (JAXA). The primary objective of GPM is to provide

high-resolution spatiotemporal precipitation information worldwide. Building on the strengths of the Tropical Rainfall Measuring Mission (TRMM) in detecting precipitation in tropical regions, GPM is equipped with two key sensors—the Dual-frequency Precipitation Radar (DPR) and the GPM Microwave Imager (GMI)—which significantly enhance the detection capability for solid precipitation and light rainfall. The Level-3 precipitation product, GPM-IMERG, provides quasi-global coverage from 50° N to 50° S and 60° N to 60° S at a spatial resolution of 0.1° × 0.1° and a temporal resolution of 30 min [8,30]. The GSMaP precipitation product is a global satellite precipitation mapping product developed by JAXA. This series includes near-real-time products (GSMaP_NRT), microwave-infrared fused products (GSMaP_MVK), and gauge-corrected products incorporating global rain gauge observations, climate, and topographic information (GSMaP_Gauge). It features high temporal resolution (1 h) and a spatial resolution of 0.10°, covering a quasi-global region from 60° N to 60° S [31,32]. The CMORPH-BLD precipitation product is a real-time satellite precipitation retrieval product developed by the NOAA Climate Prediction Center (CPC). Instead of relying solely on statistical relationships, it employs a "motion vector" method to estimate precipitation, thereby preserving the spatiotemporal continuity of precipitation distribution to a certain extent [33,34]. The reanalysis data are derived from the fifth-generation global climate product released by the European Center for Medium-Range Weather Forecasts (ECMWF). Compared with the fourth-generation reanalysis product ERA-Interim, ERA5 offers significantly improved spatiotemporal resolution. The Integrated Forecasting System (IFS) has been upgraded from Cy31r2 to Cy41r2, and the 4D-Var data assimilation method is used for the first time to integrate 10 ensemble members, assimilating many state-of-the-art instrumental datasets, including IASI, ASCAT, MWHS-2, TMI, SSMIS, AMSR-2, and GMI [35]. The forementioned precipitation datasets represent some of the most widely used satellite observation products and reanalysis precipitation products, characterized by high accuracy, stability, and long time series. Many researchers have conducted various evaluations and error analyses of these precipitation products, confirming their applicability in China [36–38].

Additionally, auxiliary parameters (elevation, slope, longitude, and latitude) were incorporated into the merging experiment to adjust for biases [39]. The digital elevation model (DEM) was derived from the Shuttle Radar Topography Mission (SRTM) conducted by NASA, with a spatial resolution of 90 m [40]. Topographic variables such as slope, longitude, and latitude were extracted from the DEM data.

To unify the spatial resolution to 0.1° and the temporal scales to daily and monthly, these precipitation products were interpolated using the Kriging method. The original data were accumulated to obtain daily and monthly scales. Table 1 presents detailed information on the datasets used in this study.

Table 1. Summary of data products used in the study.

Products	Timescale	Resolution	Download Source
ERA5	1 January 2022–31 December 2024	1-h, 0.25°	https://cds.climate.copernicus.eu/ (accessed on 26 March 2025.)
GPM-IMERG	1 January 2022–31 December 2024	30-min, 0.1°	https://gpm.nasa.gov/data (accessed on 1 April 2025.)
GSMAP-Gauge	1 January 2022–31 December 2024	1-h, 0.1°	https://sharaku.eorc.jaxa.jp/ (accessed on 26 March 2025.)
CMORPH-BLD	1 January 2022–31 December 2024	1-h, 0.25°	https://www.ncei.noaa.gov/ (accessed on 26 March 2025.)
DEM	—	90 m, --	https://www.gscloud.cn/ (accessed on 1 April 2025.)
Gauge observations	1 January 2022–31 December 2024	--, Daily	Sichuan Provincial Meteorological Service (accessed on 1 April 2025.)

3. Method

3.1. Satellite Data Evaluation Methodology

3.1.1. Multi-Timescale Accuracy Assessment of Precipitation Products

To evaluate the accuracy of the four precipitation products in the Jinsha River Basin, daily precipitation observations from 1800 automatic weather stations were used as validation data. Accuracy analysis and precipitation detection capability assessments were conducted at daily and monthly scales. The nearest neighbor method was used for spatiotemporal matching between precipitation products and station observation data. For monthly-scale evaluation, stations with more than ten missing days in a month were excluded. Daily-scale precipitation products were further evaluated across different precipitation intensity levels according to the classification standards of the People's Republic of China (2012) [41]. Table 2 presents the classification thresholds for light rain, moderate rain, heavy rain, and rainstorm based on ground-observed daily precipitation (p).

Table 2. Classification of daily precipitation intensity grades.

Precipitation Intensity	Quantitative Evaluation Threshold (mm)	Qualitative Evaluation Threshold (mm)
Light Rain	$0.1 < p < 10$	$0.1 < p < 10$
Moderate Rain	$10 < p < 25$	$10 < p < 25$
Heavy Rain	$25 < p < 50$	$25 < p < 50$
Rainstorm	$p > 50$	$p > 50$

3.1.2. Spatial Distribution Comparison and Accuracy Evaluation

To explore the spatial distribution and error characteristics of various precipitation products in the Jinsha River Basin, station precipitation data were interpolated to a 0.1° resolution grid using the Kriging method for comparison of the four products' spatial precipitation distributions. Additionally, 100 national automatic weather stations within the study area were selected to evaluate the precipitation product accuracy and precipitation event detection capability over the period from 1 January 2022 to 31 December 2024, to verify spatial error.

3.1.3. Accuracy Evaluation Metrics

Evaluation metrics are categorized into quantitative and qualitative indicators. The quantitative evaluation indicators include the correlation coefficient (CC), bias (BIAS), and root mean square error (RMSE). CC measures the correlation between precipitation products and station observations, while RMSE and BIAS quantify the root mean square error and systematic bias, respectively. The qualitative evaluation indicators comprise the probability of detection (POD), false alarm rate (FAR), and critical success index (CSI), which assess the ability of precipitation products to detect precipitation events. POD represents the probability that both the precipitation product and the ground station detect a precipitation event. FAR indicates the probability that the precipitation product detects an event while the ground station does not. CSI is a comprehensive metric that accounts for hit, false alarm, and miss rates. A precipitation event is defined as daily precipitation exceeding 0.1 mm [23,42]. Table 3 provides the formulas for these metrics.

Table 3. Evaluation metric formulas.

Category	Metric	Equation	Description
Quantitative	CC	$1-\frac{\sum_i(S_i-G_i)}{\sum_i(G_i-\mathrm{mean}(G_i))}$	Correlation coefficient
	RMSE	$\sqrt{\frac{1}{m}\sum_{i=1}^{m}(S_i-G_i)^2}$	Root mean square error
	BIAS	$\frac{\sum_i S_i}{\sum_i G_i}-1$	Bias
Qualitative	POD	$\frac{H}{H+M}$	Hit rate
	FAR	$\frac{F}{H+F}$	False alarm rate
	CSI	$\frac{H}{H+F+M}$	Critical success index

where S_i represents the i-th sample of the estimated precipitation dataset, G_i represents the i-th sample of the ground validation dataset, m is the total number of samples, H is the number of correctly detected precipitation events, F is the number of false alarms, and M is the number of missed events.

3.2. Merging Model Training

To obtain more accurate precipitation data in the Jinsha River Basin, a multi-source precipitation data merging experiment was conducted using GPM-IMERG, CMORPH-BLD, GSMAP-Gauge satellite products, ERA5 reanalysis data, and station observation data. The four precipitation products were spatiotemporally matched with the station data. Considering the influence of terrain on precipitation estimation, elevation, longitude, and latitude were incorporated as auxiliary parameters to model relationships between satellite data, reanalysis data, auxiliary parameters, and station observations. The XGBoost method (eXtreme Gradient Boosting) was used to fit the statistical relationships between the input and output parameters. XGBoost, proposed by Chen et al. [43], is an ensemble learning algorithm based on the boosting framework. It improves upon the gradient boosting decision tree (GBDT) algorithm by iteratively fitting residuals with newly generated trees, with final predictions obtained by summing the outputs of all leaf nodes. This algorithm effectively captures the nonlinear relationships between the surface precipitation observations, precipitation product data, and surface auxiliary parameters.

First, the precipitation product data were resampled to a spatial resolution of 0.1° using the Kriging interpolation method, and all hourly observation data were aggregated to the daily scale to form daily precipitation product data. For the daily ground station precipitation data, we screened the stations, eliminating those with more than 10 days of missing measurements within a single month. Using the nearest distance method, each meteorological station was matched with the nearest precipitation grid cell and terrain parameters to form a sample dataset. Then, the model was validated using fivefold cross-validation. All sample data were randomly shuffled and divided into five groups. One group served as the test dataset, and the remaining four groups served as the training datasets. The training dataset was fed into the XGBoost algorithm. A grid search strategy was employed to iteratively optimize each hyperparameter within a predefined range, and regularization terms were introduced to constrain model complexity. The model was evaluated on the test dataset using RMSE, where a smaller RMSE indicates a better model fit. Through fivefold cross-validation, five models were obtained, and the one with the smallest RMSE was selected. After iteratively adjusting the parameters to obtain the optimal model, the processed grid data were input into the model to generate a high-precision merged precipitation dataset at 0.1° resolution. The data merging experimental process is illustrated in Figure 2.

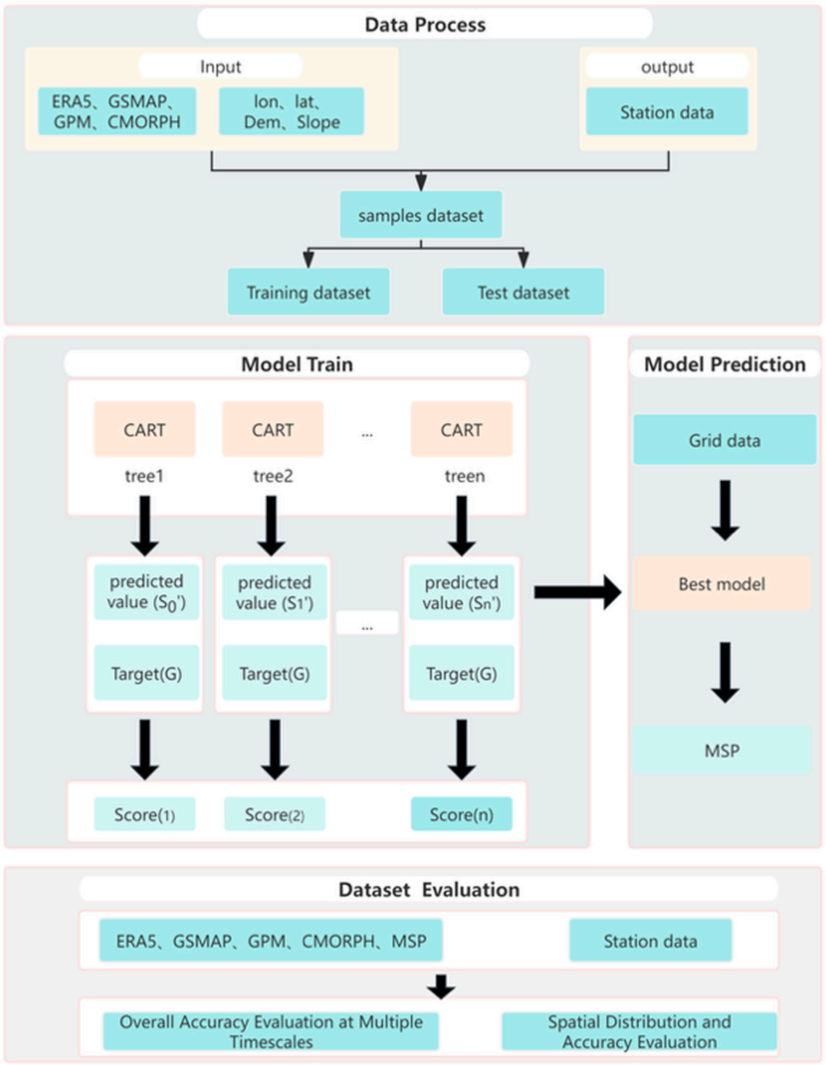

Figure 2. Flowchart of the data merging experiment.

4. Results

4.1. Multi-Timescale Precipitation Data Evaluation

4.1.1. Overall Accuracy Evaluation at Multiple Timescales

To investigate the error characteristics of several mainstream precipitation products in the Jinsha River Basin, this study conducted a comprehensive evaluation of the daily cumulative precipitation from GPM-IMERG, CMORPH-BLD, GSMAP-Gauge, ERA5, and the merged precipitation product over the period 2022–2024, using ground-based station observations as the reference truth. This study verified the overall detection accuracy of each precipitation product in the basin, as well as the improvement achieved by the merged precipitation product in terms of data accuracy. The results are presented in Table 4 and Figure 3.

Table 4. Evaluation of the daily-scale precipitation products.

Dataset	CC	RMSE	BIAS (%)	POD	FAR	CSI
GPM	0.66	4.63	11.04	0.82	0.41	0.52
ERA5	0.54	5.23	35.73	0.95	0.50	0.49
CMORPH	0.67	5.64	13.95	0.72	0.28	0.57
GSMAP	0.66	4.45	16.5	0.88	0.35	0.59
MSP	0.9	2.44	4.35	0.95	0.34	0.63

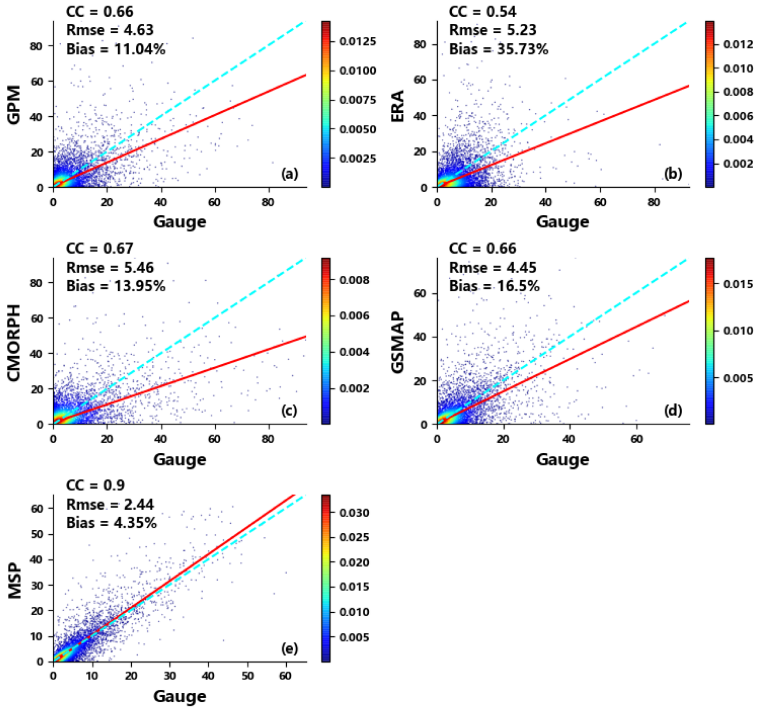

Figure 3. Regression analysis of daily-scale precipitation products with the station observations. (**a**) presents the correlation analysis between GPM-IMERG precipitation products and the station observations; (**b**) presents the correlation analysis between ERA5 precipitation products and the station observations; (**c**) presents the correlation analysis between CMORPH-BLD precipitation products and the station observations; (**d**) presents the correlation analysis between GSMAP-Gauge precipitation products and the station observations; (**e**) presents the correlation analysis between merged precipitation products and the station observations. (point density indicated by color).

Figure 3 and Table 4 present the daily-scale evaluation results for the four precipitation products and the merged dataset. A notable performance gap existed between the original products and the merged product. Bias indicators revealed that all four products tended to overestimate precipitation. Quantitative results for CMORPH-BLD, GPM-IMERG, and GSMAP-Gauge were comparable. GPM-IMERG achieved a CC of 0.66, RMSE of 4.63 mm, and BIAS of 11.04%. CMORPH-BLD yielded a CC of 0.67, RMSE of 5.46 mm, and BIAS of 13.95%. GSMAP-Gauge achieved a CC of 0.66, RMSE of 4.45 mm, and BIAS of 16.5%, with POD and CSI values of 0.88 and 0.59, respectively, substantially outperforming the other two satellite products in precipitation event detection. ERA5 showed a CC of 0.54, RMSE of 5.34 mm, and BIAS of 35.69%, significantly lagging behind the other three satellite products. It indicates that the ERA5 precipitation product exhibits a relatively low correlation with the station observations, along with substantial numerical errors in its precipitation estimates. Moreover, its spatiotemporal distribution characteristics deviated considerably from the precipitation observed at ground stations. However, ERA5 exhibited a high hit rate (0.95) but also a high false alarm rate (0.50), resulting in a low CSI. While each product has distinct strengths and weaknesses in quantitative accuracy and event detection, the multi-source fused product combines their advantages, achieving superior performance across all metrics.

Figures 4 and 5 show the evaluation results for monthly cumulative data. All products exhibited good linear regression performance at the monthly scale, with CC values above 0.8 (Figure 4). GPM-IMERG, CMORPH-BLD, and GSMAP-Gauge showed similar performance. The GPM-IMERG precipitation product exhibited the best performance across all evaluation indicators, with a CC of 0.87, a BIAS of 7.28%, and an RMSE of 37.8 mm for monthly cumulative precipitation. The CMORPH-BLD precipitation product performed relatively

poorly, achieving a CC of 0.85, a BIAS of 14.93%, and an RMSE of 48.42 mm. The ERA5 reanalysis precipitation product underperformed the three satellite precipitation products across all metrics, with a CC of 0.80, a BIAS of 35.89%, and an RMSE of 63.19 mm. These results are consistent with the evaluation of the daily-scale precipitation products, further indicating that the reanalysis product is inferior to satellite precipitation products in terms of quantitative accuracy and exhibits a substantial systematic bias in precipitation amounts. A comparison of the monthly trends in evaluation indicators for monthly-scale data (Figure 5) reveals that the CC and BIAS indicators for all precipitation products exhibited superior performance during the summer period (May–September) relative to the winter period (November–March). Among these products, the ERA5 precipitation product demonstrated the most pronounced seasonal variability. Specifically, in winter, the BIAS exceeded 1 and the CC fell below 0.5, whereas in summer, the BIAS dropped below 0.8 and the CC remained approximately 0.6. However, the RMSE evaluation metric yielded more favorable values in winter than in summer. This disparity arises from the fact that total precipitation in summer is considerably higher than that in winter. As a result, the RMSE tended to increase with precipitation volume, creating a systematic difference between the evaluation outcomes for summer and winter products. Furthermore, the trends of the evaluation indicators were generally consistent across all precipitation products. Following the multi-source data merging experiment, the merged precipitation product (MSP) exhibited substantially superior performance across all evaluation metrics compared to the other products, thereby demonstrating its advantage.

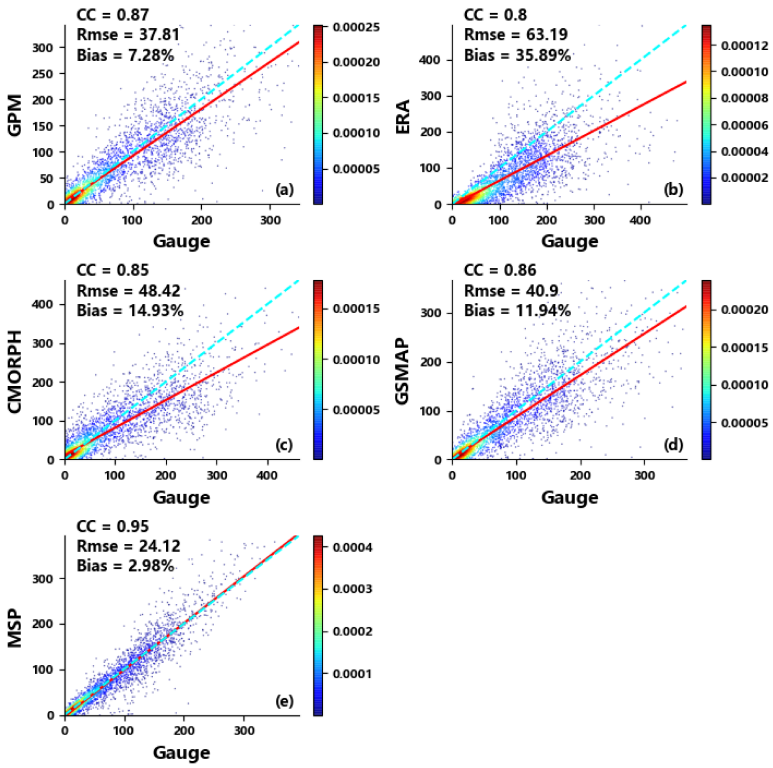

Figure 4. Regression analysis of monthly-scale precipitation products with the station observations; (**a**) presents the correlation analysis between GPM-IMERG precipitation products and the station observations; (**b**) presents the correlation analysis between ERA5 precipitation products and the station observations; (**c**) presents the correlation analysis between CMORPH-BLD precipitation products and the station observations; (**d**) presents the correlation analysis between GSMAP-Gauge precipitation products and the station observations; (**e**) presents the correlation analysis between merged precipitation products and the station observations. (point density indicated by color).

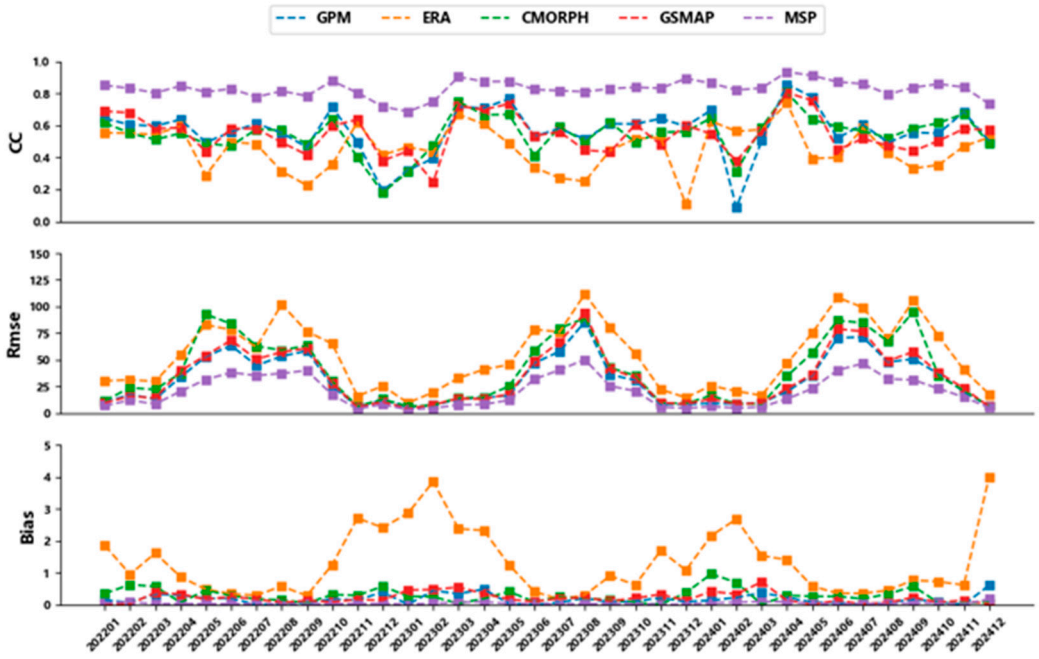

Figure 5. Monthly variation in accuracy metrics for precipitation products.

4.1.2. Accuracy Assessment Across Precipitation Intensity Ranges

To further investigate the detection effectiveness of various precipitation products for different precipitation intensity events, this study classified precipitation data into four intensity levels—light rain, moderate rain, heavy rain, and torrential rain—based on the ground-based station observations. For each precipitation product and each intensity level, the quantitative accuracy and precipitation event detection capability were assessed. The evaluation results are presented in Figures 6 and 7.

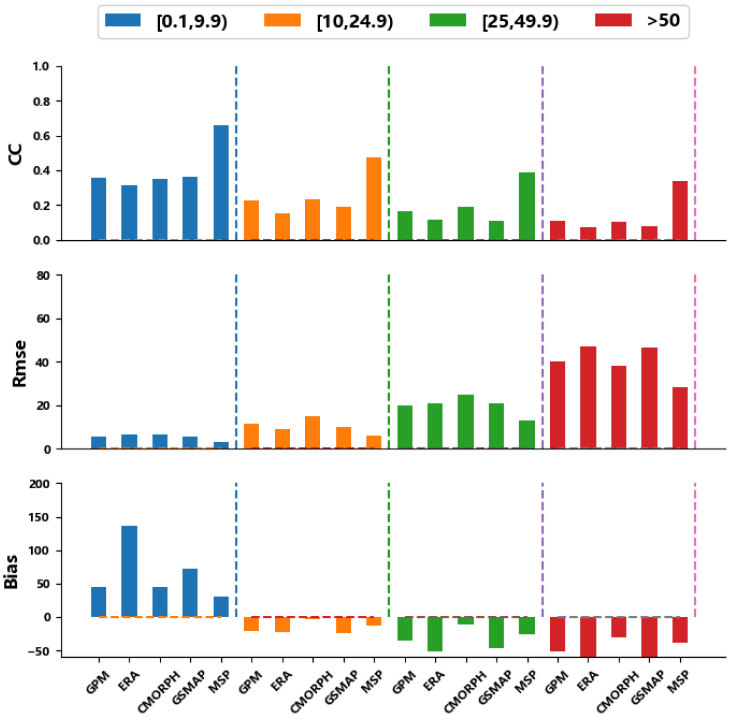

Figure 6. Quantitative accuracy evaluation across precipitation intensity ranges.

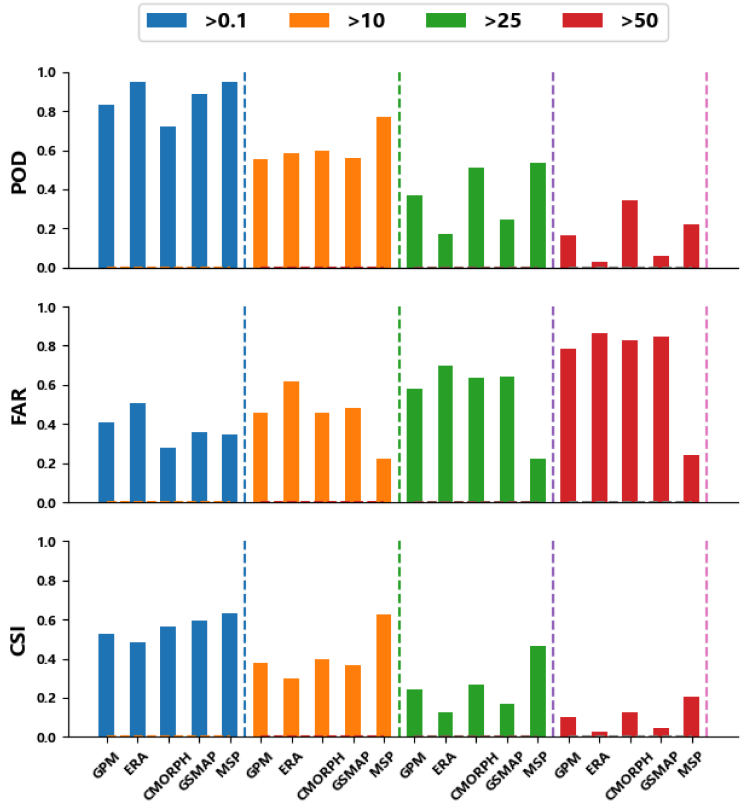

Figure 7. Precipitation event detection capability across precipitation intensity ranges.

Figure 6 presents the quantitative accuracy assessment of various precipitation products across different precipitation intensity events. In terms of the CC, both GPM-IMERG and CMORPH-BLD performed better for light, moderate, and heavy rain. ERA5 exhibited significantly poorer performance than the other three satellite precipitation products across all intensity categories. The merged precipitation product outperformed all four original precipitation products in CC evaluation across every precipitation intensity range. Overall, the correlation coefficient between the precipitation products and station observations increased as the precipitation amount decreased. RMSE results showed that GPM-IMERG performed well across categories, while ERA5 and GSMAP-Gauge performed better for moderate rain. GPM-IMERG showed weaker performance for heavy rain and rainstorm. Bias analysis revealed an overestimation of light rain and underestimation of heavy rain across products, particularly for ERA5 and GSMAP-Gauge. For precipitation > 10 mm, overestimation exceeded 50%; for precipitation > 50 mm, underestimation exceeded 50%. The merged precipitation product combined the advantages of GPM-IMERG and CMORPH-BLD, significantly mitigating the overestimation of light rainfall events and the underestimation of heavy rainfall events.

The qualitative assessment results for precipitation event detection capability are presented in Figure 7. The ERA5 and GSMAP-Gauge precipitation products exhibited relatively high hit rates for light and moderate rain events, whereas GPM-IMERG and CMORPH-BLD demonstrated better hit rates for heavy rain and torrential rain events compared to the other two products. CMORPH-BLD achieved the lowest false alarm rate across all precipitation events, resulting in a favorable critical success index (CSI). In contrast, ERA5 showed the highest false alarm rate, which significantly degraded its CSI performance. The merged precipitation product integrates the strengths of the aforementioned products, achieving a modest improvement in POD index and a substantial reduction in FAR index.

4.2. Spatial Distribution and Accuracy Evaluation

To analyze spatial patterns, daily average precipitation during the rainy season (May–September, 2022–2024) was calculated. Station data were interpolated to a 0.1° grid, and results were compared with product outputs (Figure 8).

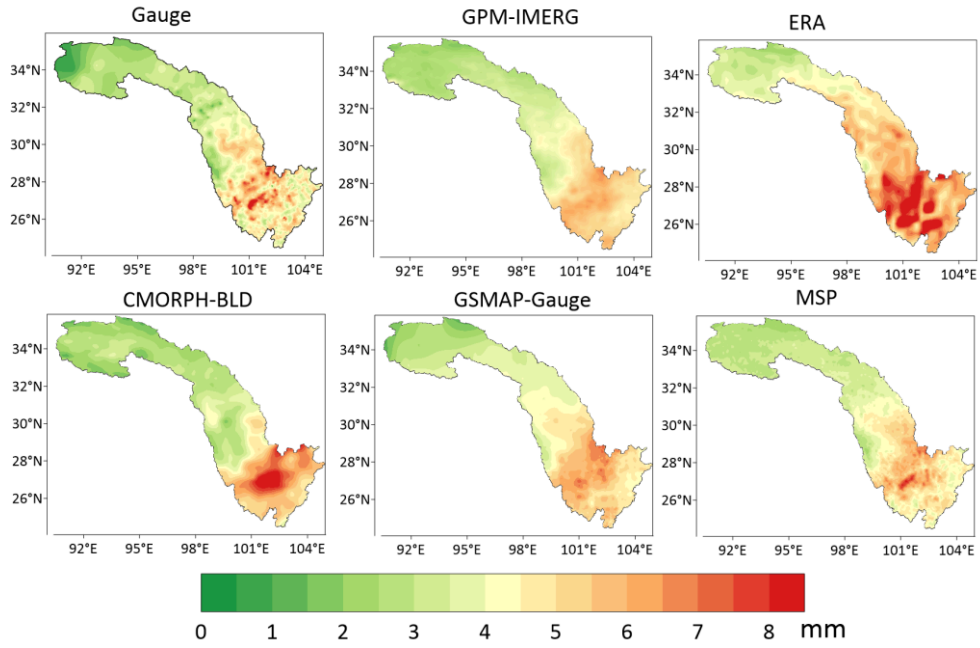

Figure 8. Spatial distribution of average daily precipitation during rainy season.

It can be observed that the spatial distribution characteristics of daily average precipitation in the Jinsha River Basin were generally consistent across the several precipitation products. Precipitation amounts exhibited an overall increasing trend from the northwest to the southeast. The southeastern area of the lower reaches, which comprises plains and basins, receives an average daily precipitation exceeding 6 mm. In contrast, the northwestern area of the upper reaches, characterized by plateaus and mountainous terrain, recorded an average daily precipitation of less than 3 mm. Compared with the ground station observations, each precipitation product showed an overestimation in the downstream area of the Jinsha River Basin and an underestimation in the upstream area. The overestimation was particularly pronounced in the ERA5 product, especially over a large area in the lower reaches of the eastern low-altitude basin. The GSMAP-Gauge product exhibited spatial distribution characteristics similar to those of GPM-IMERG, but its overestimation in the downstream area was weaker than that of GPM-IMERG, and both products showed a slight underestimation in the upstream area. Relative to GPM-IMERG and GSMAP-Gauge, the CMORPH-BLD product displayed spatial precipitation distribution characteristics more closely resembling those of the ground station observations. However, it exhibited significant overestimation in the downstream area, with a higher magnitude than that of GSMAP-Gauge and GPM-IMERG. The precipitation spatial distribution derived from the merged precipitation product was the closest to the station-observed distribution. Moreover, it effectively corrected the overestimation in the downstream area and the underestimation in the upstream area observed in the original precipitation products.

To quantitatively evaluate spatial accuracy, 100 national automatic weather stations were selected as validation points (Figure 9).

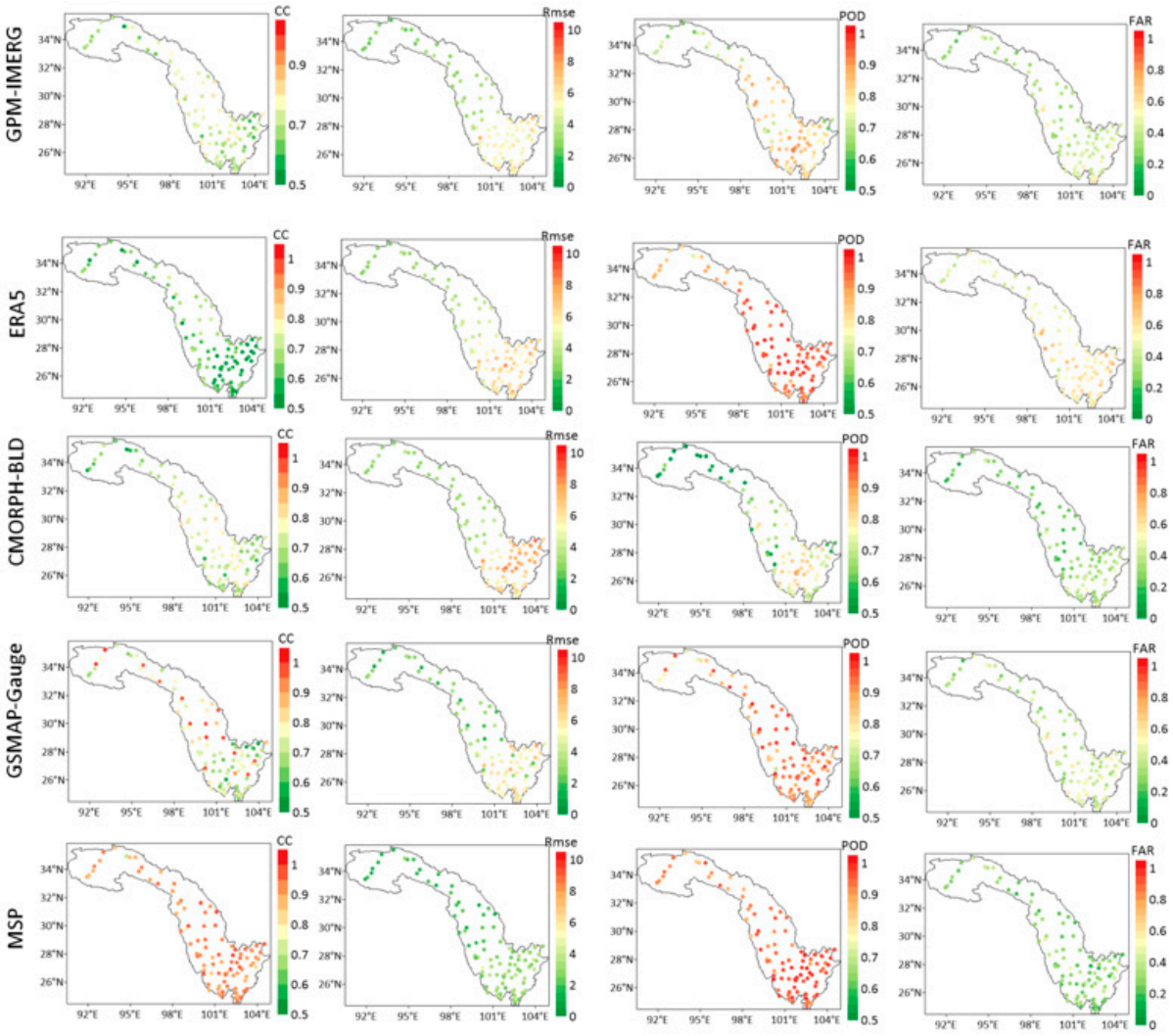

Figure 9. Accuracy evaluation results at 100 national automatic weather stations.

CC, POD, and FAR evaluations showed better performance in downstream regions than upstream regions. RMSE was higher downstream due to greater precipitation totals. The merged precipitation product improved upstream CC and reduced downstream RMSE. GPM-IMERG and CMORPH-BLD achieved CC values around 0.7 at most stations. GSMAP-Gauge showed similar performance, with higher correlation at some stations due to its integration of multiple satellite and station data. ERA5 CC was generally below 0.6. The merged precipitation product raised the CC to >0.8 at most stations. CMORPH-BLD and ERA5 showed the highest RMSE, particularly downstream (>6 mm), while GSMAP-Gauge had the lowest RMSE (<5 mm). The merged precipitation product achieved RMSE values around 3 mm. In terms of precipitation event detection (POD), the ERA5 and GSMAP-Gauge products achieved the highest scores, followed by GPM-IMERG, with CMORPH-BLD ranking the lowest. Overall, the hit rate in the northwestern upper reached was relatively low, with POD values at most stations falling below 0.8. After the merging experiment, the hit rate in this region improved markedly. Regarding the false alarm rate (FAR), the ERA5 and GPM-IMERG precipitation products exhibited higher values, whereas CMORPH-BLD and GSMAP-Gauge showed relatively lower false alarm rates. The merged precipitation product achieved the lowest FAR, demonstrating substantially better performance than all four original precipitation products.

4.3. Discussion

This study addresses the lack of high-precision gridded precipitation data in the complex terrain of the Jinsha River Basin. Using multiple satellite-based precipitation products (GPM-IMERG, CMORPH-BLD, GSMAP-Gauge) and the global reanalysis product ERA5, along with ground-based station precipitation measurements as a reference, a multi-source precipitation data merging experiment was conducted integrating satellite, reanalysis, and station data. As a result, a multi-source merged precipitation dataset at 0.1° spatial resolution and daily temporal resolution was obtained for the Jinsha River Basin.

First, the error characteristics of the aforementioned precipitation products were comprehensively analyzed. The results showed that the overall accuracy of the GPM-IMERG, GSMaP-Gauge, and CMORPH-BLD products at daily and monthly scales exhibited no significant differences. In contrast, the ERA5 reanalysis product performed poorly in terms of correlation and root mean square error, indicating a substantial systematic bias within the Jinsha River Basin (Figures 3 and 4). The detection accuracy of the four precipitation products exhibited generally consistent temporal trends. For the CC and BIAS indicators, all products performed better in summer (May–September) than in winter (November–March). In contrast, the RMSE indicator yielded better performance in winter than in summer. This discrepancy arises because the total precipitation volume in summer is substantially higher than that in winter, and RMSE increases with precipitation amount, leading to a notable gap between the evaluation values for summer and winter precipitation products (Figure 5).

Secondly, this study categorized precipitation events of different intensities based on daily rainfall amounts to further investigate the detection performance of various precipitation products under varying intensity conditions. Quantitative accuracy analysis showed that the detection differences among the GPM-IMERG, GSMAP-Gauge, and CMORPH-BLD satellite precipitation products were relatively small, whereas the ERA5 product performed worse than these three satellite-based products across all intensity levels (Figure 6). In terms of qualitative detection for different precipitation intensities, the overall results indicated that ERA5 and GSMAP-Gauge performed better in detecting light rain events (daily precipitation < 10 mm), whereas CMORPH-BLD and GPM-IMERG outperformed the other two products in terms of hit rates for heavy and torrential rain events (daily precipitation > 25 mm) (Figure 7). The ERA5 precipitation product assimilates ground-based observations, satellite radiances, radiosonde measurements, and other data into a global numerical weather prediction model. For weak precipitation events, its simulations rely primarily on parameterized representations of stratiform cloud microphysical processes. Such precipitation typically manifests as stable, continuous, and widespread processes, which are relatively easier for models to capture. However, this leads to an overestimation of the frequency of weak precipitation, resulting in a significantly higher false alarm rate compared to the satellite precipitation products. Additionally, the model's parameterization schemes for convective processes introduce spatial smoothing effects. Extreme localized heavy rainfall events may be averaged into moderate precipitation over coarse model grids, thereby suppressing peak rainfall values and failing to capture intense downpours [44]. GSMAP-Gauge combines microwave retrieval with ground-based gauge calibration. Light rainfall often originates from warm-cloud processes (with cloud-top temperatures above 0 °C), involving few ice-phase particles and extremely weak microwave scattering signals. Under such conditions, the sensitivity of satellite microwave retrievals decreases, making them heavily dependent on ground-based rain gauge data [45]. CMORPH-BLD and GPM-IMERG are global high-spatiotemporal-resolution precipitation datasets developed using multiple microwave and infrared data sources. Intense precipitation is invariably

associated with deep convective clouds, where strong updrafts lift water droplets above the freezing level, forming abundant ice crystals, graupel, hailstones, and other ice-phase particles. These ice-phase particles strongly scatter high-frequency microwave signals, causing significant reductions in the brightness temperature received by satellites. Precipitation retrieval based on the correlation between multi-channel brightness temperatures and precipitation intensity has a clear physical basis and low misclassification rates, enabling a more accurate capture of instantaneous peak intensities during convective precipitation events [46].

Finally, the spatial distribution characteristics and error patterns of several precipitation products over the Jinsha River Basin were analyzed. The daily average precipitation distributions of these products were generally consistent, exhibiting an overall increasing trend from the northwest to the southeast. Precipitation errors were characterized by overestimation in the lower reaches and underestimation in the upper reaches of the basin. Following the multi-source precipitation merging experiment, the accuracy metrics of the merged product were significantly improved, and its spatial distribution of precipitation closely resembled that of the station observations. This effectively corrected the overestimation in the downstream area and the underestimation in the upstream area observed in the original precipitation products. An evaluation of each precipitation product at different stations within the Jinsha River Basin revealed that the accuracy in the downstream area was higher than that in the upstream area. The merged precipitation product substantially enhanced data accuracy in the upstream region; nevertheless, its accuracy remained lower than that in the downstream region. This discrepancy arises because the ability of original satellite data to detect ground precipitation is influenced by topographic factors such as altitude and slope, which in turn introduces certain biases into the relationship between the multi-source precipitation merging product and station-based measurements. Related studies have indicated that in higher-altitude areas, multi-source precipitation merged products exhibit greater instability in precipitation estimation [47].

5. Conclusions

To obtain high-precision, high-spatiotemporal-resolution precipitation data for the Jinsha River Basin, this study evaluated the accuracy and precipitation event detection capability of several mainstream satellite precipitation products and reanalysis data. Using machine learning and accounting for topographic influences, a multi-source precipitation merging experiment was conducted. The main conclusions are as follows:

(1). GSMAP-Gauge demonstrates strong performance in both quantitative accuracy and event detection. CMORPH-BLD and GPM-IMERG show good correlation with station data but weaker event detection. ERA5 exhibits high hit rates but also high false alarm rates, with poor quantitative accuracy.

(2). Different products excel in detecting precipitation events across different intensity ranges. The quantitative accuracy of the ERA5 precipitation product is inferior to that of the three satellite-based precipitation products across all precipitation intensity levels. ERA5 and GSMAP-Gauge perform better for light rain (<10 mm/day), while CMORPH-BLD and GPM-IMERG show higher hit rates for heavy rain and rainstorm (>25 mm/day).

(3). Spatial precipitation distributions of the products are generally consistent with station observations. The fused product aligns more closely with station data and shows substantial improvements in all accuracy metrics.

In summary, this study produced a daily-scale precipitation dataset for the Jinsha River Basin (2022–2024) at 0.1° spatial resolution by fusing multi-source precipitation products with topographic auxiliary parameters using a machine learning algorithm. Compared with the original products, the fused dataset showed significant improvements in both

quantitative and qualitative evaluations: CC increased from 0.67 to 0.9, RMSE decreased from 5.64 mm to 2.44 mm, POD increased from 0.95 to 0.96, and CSI increased from 0.59 to 0.63, demonstrating the feasibility of the merging approach. Future research could incorporate additional multi-source precipitation data (e.g., weather radar) to further enhance accuracy and expand spatiotemporal resolution. Developing hourly (or sub-hourly) and kilometer-scale (or sub-kilometer) precipitation products would be of great significance for studying precipitation characteristics over complex terrain in the Jinsha River Basin.

Author Contributions: The authors of this study contributed as follows: Y.Y. was responsible for Conceptualization, Data Curation, Formal Analysis, Investigation, Methodology, Software, Writing—Original Draft, and Writing—Review & Editing; H.W. contributed to Data Curation, Investigation, Project Administration, Resources, Supervision, Validation, and Visualization; H.Z. led Conceptualization, Formal Analysis, Funding Acquisition, Investigation, Methodology, and Project Administration; N.Z. participated in Investigation, Supervision, Validation, and Visualization; C.C. contributed to Investigation, Supervision, Validation, and Visualization; and C.X. was involved in Investigation, Supervision, and Validation. All authors have read and agreed to the published version of the manuscript.

Funding: This work was sponsored by The Three Gorges Jinsha River Chuanyun Hydropower Development Co., Ltd. (4324020002).

Data Availability Statement: The data employed in this study are openly accessible. The procedure for loading these data is presented in Table 1.

Acknowledgments: We would like to express our heartfelt gratitude to the Sichuan Meteorological Bureau, National Aeronautics and Space Administration, National Oceanic Atmospheric Administration, European Center for Medium-Range Weather Forecasts, and the Japan Aerospace Exploration Agency for providing the data used in this study. Additionally, we extend our appreciation to the reviewers for their valuable feedback and insightful suggestions, which significantly contributed to enhancing the quality of this manuscript.

Conflicts of Interest: Yin Ye, Wang HanTao, Zhang Hui, Zhao NanShan, and Cheng CuiHua were employed by the company "The Three Gorges Jinsha River Chuanyun Hydropower Development Co., Ltd.". Xie ChengHua was employed by the company "Chengdu Yuanwang Detection Technology Co., Ltd.". The authors declare that this study received funding from "The Three Gorges Jinsha River Chuanyun Hydropower Development Co., Ltd.". The funder had the following involvement with the study: the funder provided the research ideas, data, and project administration.

References

1. Yan, Y.; Wang, H.; Li, G.; Xia, J.; Ge, F.; Zeng, Q.; Ren, X.; Tan, L. Projection of Future Extreme Precipitation in China Based on the CMIP6 from a Machine Learning Perspective. *Remote Sens.* **2022**, *14*, 4033. [CrossRef]
2. Taylor, C.M.; Jeu, R.A.M.D.; Guichard, F.; Harris, P.P.; Dorigo, W.A. Afternoon Rain More Likely over Drier Soils. *Nature* **2012**, *489*, 423–426. [CrossRef] [PubMed]
3. Song, Y.; Liu, H.; Wang, X.; Zhang, N.; Sun, J. Numerical Simulation of the Impact of Urban Non-Uniformity on Precipitation. *Adv. Atmos. Sci.* **2016**, *33*, 783–793. [CrossRef]
4. Shrestha, M.; Artan, G.A.; Bajracharya, S.; Sharma, R.R. Using satellite-based rainfall estimates for streamflow modelling: Bagmati Basin. *J. Flood Risk Manag.* **2008**, *1*, 89–99. [CrossRef]
5. Antal, A.; Guerreiro, P.M.; Cheval, S. Comparison of spatial interpolation methods for estimating the precipitation distribution in Porfugal. *Theor. Appl. Climatol.* **2021**, *145*, 1193–1206. [CrossRef]
6. Pereira, P.; Oliva, M.; Misiune, I. Spatial intelpolation of precipitation indexes in Sierra Nevada(Spain): Comparing the performance of some interpolation methods. *Theor. Appl. Climatol.* **2016**, *126*, 683–698.
7. Derin, Y.; Yilmaz, K.K. Evaluation of multiple satellite-based precipitation products over complex topography. *J. Hydrometeorol.* **2014**, *15*, 1498–1516. [CrossRef]

8. Wang, H.; Tan, L.; Zhang, F.; Zheng, J.; Liu, Y.; Zeng, Q.; Yan, Y.; Ren, X.; Xiang, J. Three-Dimensional Structure Analysis and Droplet Spectrum Characteristics of Southwest Vortex Precipitation System Based on GPM-DPR. *Remote Sens.* **2022**, *14*, 4063. [CrossRef]
9. Yoon, S.S.; Lim, S.H. Analyzing the Application of X-Band Radar for Improving Rainfall Observation and Flood Forecasting in Yeongdong, South Korea. *Remote Sens.* **2021**, *14*, 43. [CrossRef]
10. Sungmin, O.; Foelsche, U.; Kirchengast, G.; Fuchsberger, J.; Tan, J.; Petersen, W.A. Evaluation of GPM IMERG Early, Late, and Final rainfall estimates using WegenerNet gauge data in southeastern Austria. *Hydrol. Earth Syst. Sci.* **2017**, *21*, 72–89. [CrossRef]
11. Zhang, D.R.; Birgisson, B.; Luo, X. A new dynamic modulus predictive model for asphalt mixtures based on the law of mixtures. *Constr. Build. Mater.* **2020**, *255*, 119348. [CrossRef]
12. Wang, H.; Li, Z.; Zhang, T.; Chen, Q.; Guo, X.; Zeng, Q.; Xiang, J. Downscaling of GPM satellite precipitation products based on machine learning method in complex terrain and limited observation area. *Adv. Space Res.* **2023**, *72*, 2226–2244. [CrossRef]
13. Nan, T.; Chen, J.; Ding, Z.; Li, W.; Chen, H. Deep learning-based multi-source precipitation merging for the Tibetan Plateau. *Sci. China Earh Sci.* **2023**, *66*, 852–870. [CrossRef]
14. Zeng, S.; Yong, B. Evaluation of the GPM-based IMERG and GSMaP Precipitation estimates over the Sichuan region. *Acta Geogr. Sin.* **2019**, *74*, 1305–1318. (In Chinese)
15. Xu, T.; Gu, J.; Liang, L.; Guan, H.; Cao, Y.; Gong, J. Applicability assessment of various satellite precipitation product Jinsha River Basin. *Yangtze River* **2025**, *56*, 112–120. (In Chinese) [CrossRef]
16. Uppala, S.; Dee, D.; Kobayashi, S.; Berrisford, P.; Simmons, A. Towards a climate data assimilation system: Status update of ERA-Interim. *ECMWF Newsl.* **2008**, *115*, 12–18.
17. Wang, C.X.; Graham, R.M.; Wang, K.G.; Gerland, S.; Granskog, M.A. Comparison of ERA5 and ERA-Interim near-surface air temperature, snowfall and precipitation over Arctic sea ice: Effects on sea ice thermodynamics and evolution. *Cryosphere* **2019**, *13*, 1661–1679. [CrossRef]
18. Kidd, C.; Bauer, P.; Turk, J.; Huffman, G.J.; Joyce, R.; Hsu, K.L.; Braithwaite, D. Intercomparison of high-resolution precipitation products over northwest Europe. *J. Hydrometeorol.* **2012**, *13*, 67–83. [CrossRef]
19. Chao, L.; Zhang, K.; Li, Z.; Zhu, Y.; Wang, J.; Yu, Z. Geographically Weighted Regression Based Methods for Merging Satellite and Gauge Precipitation. *J. Hydrol.* **2018**, *558*, 275–289. [CrossRef]
20. Pan, Y.; Shen, Y.; Yu, J.; Zhao, P. Analysis of the combined gauge—Satellite hourly precipitation over China based on the OI technique. *Acta Meteorol. Sin.* **2012**, *70*, 1381–1389. (In Chinese)
21. Yang, P.; Ng, T.L. Fast Bayesian Regression Kriging Method for Real-Time Merging of Radar, Rain Gauge, and Crowdsourced Rainfall Data. *Water Resour. Res.* **2019**, *55*, 3194–3214. [CrossRef]
22. Wu, H.; Yang, Q.; Liu, J.; Wang, G. A Spatiotemporal Deep Fusion Model for Merging Satellite and Gauge Precipitation in China. *J. Hydrol.* **2020**, *584*, 124664. [CrossRef]
23. Li, Z.; Wang, H.; Zhang, T.; Zeng, Q.; Xiang, J.; Liu, Z.; Yang, R. Multi-Source Precipitation Data Merging for High-Resolution Daily Rainfall in Complex Terrain. *Remote Sens.* **2023**, *15*, 4345. [CrossRef]
24. Xia, X.L.; Liu, Y.X.Y.; Jing, W.L.; Yao, L. Assessment of Four Satellite-Based Precipitation Products Over the Pearl River Basin, China. *IEEE Access* **2021**, *9*, 46–65. [CrossRef]
25. Brocca, L.; Ciabatta, L.; Massari, C.; Moramarco, T.; Hahn, S.; Hasenauer, S.; Kidd, R.; Dorigo, W.; Wagner, W.; Levizzani, V. Soil as a natural rain gauge: Estimating global rainfall from satellite soil moisture data. *J. Geophys. Res.-Atmos.* **2014**, *119*, 41–60. [CrossRef]
26. Tan, M.L.; Ibrahim, A.L.; Duan, Z.; Cracknell, A.P.; Chaplot, V. Evaluation of Six High-Resolution Satellite and Ground-Based Precipitation Products over Malaysia. *Remote Sens.* **2015**, *7*, 1504–1528. [CrossRef]
27. Sharifi, E.; Eitzinger, J.; Dorigo, W. Performance of the State-Of-The-Art Gridded Precipitation Products over Mountainous Terrain: A Regional Study over Austria. *Remote Sens.* **2019**, *11*, 2018. [CrossRef]
28. Brocca, L.; Moramarco, T.; Melone, F.; Wagner, W. A new method for rainfall estimation through soil moisture observations. *Geophys. Res. Lett.* **2013**, *40*, 833–853. [CrossRef]
29. Zubieta, R.; Getirana, A.; Espinoza, J.C.; Lavado-Casimiro, W.; Aragon, L. Hydrological modeling of the Peruvian-Ecuadorian Amazon Basin using GPM-IMERG satellite-based precipitation dataset. *Hydrol. Earth Syst. Sci.* **2017**, *21*, 3543–3555. [CrossRef] [PubMed]
30. Wang, Z.; Zhong, R.; Lai, C.; Chen, J. Evaluation of the GPM IMERG satellite-based precipitation products and the hydrological utility. *Atmos. Res.* **2017**, *196*, 151–163. [CrossRef]
31. Tian, Y.; Peters-Lidard, C.D.; Adler, R.F.; Kubota, T.; Ushio, T. Evaluation of GSMaP Precipitation Estimates over the Contiguous United States. *J. Hydrometeorol.* **2010**, *11*, 566–574. [CrossRef]
32. Zhou, Z.; Guo, B.; Xing, W.; Zhou, J.; Xu, F.; Xu, Y. Comprehensive evaluation of latest GPM era IMERG and GSMaP precipitation products over mainland China. *Atmos. Res.* **2020**, *246*, 105132. [CrossRef]

33. Nogueira, M. Inter-comparison of ERA-5, ERA-interim and GPCP rainfall over the last 40 years: Process-based analysis of systematic and random differences. *J. Hydrol.* **2020**, *583*, 124632. [CrossRef]
34. Lu, J.; Jia, L.; Menenti, M.; Yan, Y.; Zheng, C.; Zhou, J. Performance of the Standardized Precipitation Index Based on the TMPA and CMORPH Precipitation Products for Drought Monitoring in China. *IEEE J. Sel. Top. Appl. Earth Obs. Remote Sens.* **2018**, *11*, 1387–1396. [CrossRef]
35. Lei, X.; Xu, W.; Chen, S.; Yu, T.; Hu, Z.; Zhang, M.; Jiang, L. How Well Does the ERA5 Reanalysis Capture the Extreme Climate Events Over China? Part I: Extreme Precipitation. *Front. Environ. Sci.* **2022**, *10*, 921658. [CrossRef]
36. Lu, D.K.; Yong, B. Evaluation and hydrological utility of the latest GPM IMERG V5 and GSMaP V7 precipitation products over the Tibetan Plateau. *Remote Sens.* **2018**, *10*, 2022. [CrossRef]
37. Zhang, S.J.; Wang, D.H.; Qin, Z.K.; Zheng, Y.; Guo, J. Assessment of the GPM and TRMM precipitation products using the rain gauge network over the Tibetan Plateau. *J. Meteorol. Res.* **2018**, *32*, 324–336. [CrossRef]
38. Zhao, P.; He, Z.; Ma, D.; Wang, W. Evaluation of ERA5-Land reanalysis datasets for extreme temperatures in the Qilian Mountains of China. *Front. Ecol. Evol.* **2023**, *11*, 1135895. [CrossRef]
39. Yan, X.; Chen, H.; Tian, B.; Sheng, S.; Kim, J.S. A Downscaling–Merging Scheme for Improving Daily Spatial Precipitation Estimates Based on Random Forest and Cokriging. *Remote Sens.* **2021**, *13*, 2040. [CrossRef]
40. Domenico, C.; Dario, G.; Marcello, S. Editorial: Advances in Quantitative Geomorphology: From DEM Analysis to Modeling of Surface Processes. *Front. Earth Sci.* **2022**, *10*, 874950. [CrossRef]
41. *GB/T 28592-2012*; Grade of Precipitation. China Standard Press: Beijing, China, 2012.
42. Yang, Z.; Hsu, K.; Sorooshian, S.; Xu, X.; Braithwaite, D.; Zhang, Y.; Verbist, K.M.J. Merging high-resolution satellite-based precipitation fields and point-scale rain gauge measurements-A case study in Chile. *J. Geophys. Res. Biogeo.* **2017**, *122*, 5267–5284. [CrossRef]
43. Chen, T.; Guestrin, C. XGBoost: A Scalable Tree Boosting System. In *KDD '16, Proceedings of the 22nd ACM SIGKDD International Conference on Knowledge Discovery and Data Mining, San Francisco, CA, USA, 13–17 August 2016*; Zhang, L., Wang, S., Zhang, X., Wang, Y., Li, B., Shen, D., Ji, S., Eds.; Association for Computing Machinery: New York, NY, USA, 2016.
44. Wang, Y.; Fu, Y. Responses of TMI channels to precipitation cloud parameters as suggested by numerical simulation. *Acta Meteorol. Sin.* **2010**, *68*, 315–324. [CrossRef]
45. Gu, H.; Shen, D.; Xiao, S.; Zhang, C.; Bai, F.; Yu, F. Evaluation of Daily and Hourly Performance of Multi-Source Satellite Precipitation Products in China's Nine Water Resource Regions. *Remote Sens.* **2024**, *16*, 1516. [CrossRef]
46. Huang, Y.; Liu, Z.; Song, W.; Wen, W. Evaluation of GPM IMERG Precipitation Product on Extreme Precipitation in the Lower Reaches of Jinsha River. *Plateau Mt. Meteorol. Res.* **2024**, *44*, 76–84. [CrossRef]
47. Bi, S.; Bi, S.; Chen, D.; Pan, J.; Wang, J. A Double-Smoothing Algorithm for Integrating Satellite Precipitation Products in Areas with Sparsely Distributed In Situ Networks. *ISPRS Int. J. Geo-Inf.* **2017**, *6*, 28. [CrossRef]